

c-Abl Tyrosine Kinase Adopts Multiple Active Conformational States in Solution

John Badger,^{†,⊥} Prerna Grover,^{‡,⊥} Haibin Shi,[‡] Shoghag B. Panjarian,^{‡,#} John R. Engen,[§] Thomas E. Smithgall,[‡] and Lee Makowski^{*,§,||}

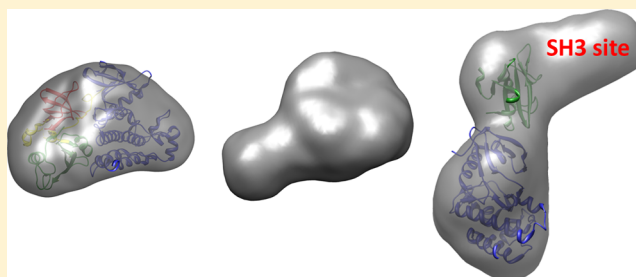
[†]DeltaG Technologies, San Diego, California 92122, United States

[‡]Department of Microbiology and Molecular Genetics, University of Pittsburgh School of Medicine, Pittsburgh, Pennsylvania 15219, United States

[§]Department of Chemistry and Chemical Biology and ^{||}Department of Bioengineering, Northeastern University, Boston, Massachusetts 02115, United States

S Supporting Information

ABSTRACT: Protein tyrosine kinases of the Abl family have diverse roles in normal cellular regulation and drive several forms of leukemia as oncogenic fusion proteins. In the crystal structure of the inactive c-Abl kinase core, the SH2 and SH3 domains dock onto the back of the kinase domain, resulting in a compact, assembled state. This inactive conformation is stabilized by the interaction of the myristoylated N-cap with a pocket in the C-lobe of the kinase domain. Mutations that perturb these intramolecular interactions result in kinase activation. Here, we present X-ray scattering solution structures of multidomain c-Abl kinase core proteins modeling diverse active states. Surprisingly, the relative positions of the regulatory N-cap, SH3, and SH2 domains in an active myristic acid binding pocket mutant (A356N) were virtually identical to those of the assembled wild-type kinase core, indicating that Abl kinase activation does not require dramatic reorganization of the downregulated core structure. In contrast, the positions of the SH2 and SH3 domains in a clinically relevant imatinib-resistant gatekeeper mutant (T315I) appear to be reconfigured relative to their positions in the wild-type protein. Our results demonstrate that c-Abl kinase activation can occur either with (T315I) or without (A356N) global allosteric changes in the core, revealing the potential for previously unrecognized signaling diversity.



The c-Abl tyrosine kinase is a modular signaling protein with multiple physiological roles ranging from regulation of the actin cytoskeleton to integration of DNA damage responses in the nucleus.^{1,2} Abl is well-known in the context of Bcr-Abl, the oncogenic tyrosine kinase responsible for chronic myelogenous leukemia (CML) and some cases of ALL.³ In CML, the normally tight regulation of c-Abl is lost as a result of fusion to Bcr sequences, and this uncontrolled kinase activity drives myeloid progenitor cell transformation and disease progression. Clinical management of CML has been revolutionized by the development of ATP-competitive inhibitors for the Abl kinase domain, of which imatinib (Gleevec) is the prototype.⁴ The selectivity of imatinib for Bcr-Abl stems in part from its ability to trap a unique inactive conformation of the kinase active site.⁵ Nevertheless, the evolution of drug-resistant mutants that affect imatinib binding has required the ongoing development of newer classes of Abl inhibitors. The so-called “gatekeeper” mutant of Bcr-Abl, in which kinase domain position Thr315 in the imatinib binding site is replaced by isoleucine (T315I mutant), has been difficult to target with small molecule inhibitors.⁶ Other work has shown that the T315I mutation enhances both c-Abl and Bcr-Abl kinase

activity, although the effect of this mutation on the overall structure and dynamics of c-Abl is less clear.^{7–9}

Crystallographic work on the inactive c-Abl kinase “core”, which consists of an N-terminal cap region (N-cap), regulatory SH2 and SH3 domains, and the kinase domain, has identified a compact, inactive conformation regulated by multiple inter-domain contacts.^{10,11} In this downregulated state, the SH2 and SH3 domains are docked onto the back of the kinase domain. Regulatory domain interactions are stabilized by addition of a myristic acid group to the N-cap, which inserts into a deep C-terminal lobe cavity unique to the Abl kinase domain. Mutations that perturb any of these intramolecular interactions lead to kinase domain activation, providing important validation of the crystal structure.¹² A model of the assembled, downregulated c-Abl core structure is presented in Figure 1A.

While X-ray crystallography has provided tremendous insight regarding the relative positions of the regulatory and catalytic domains in the downregulated state of the c-Abl core, the fate

Received: March 3, 2016

Revised: May 5, 2016

Published: May 11, 2016

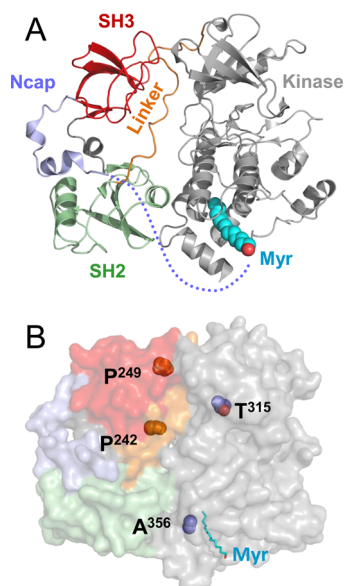


Figure 1. Intramolecular interactions regulate c-Abl structure and activity. (A) Crystal structure of the assembled, downregulated c-Abl kinase core (PDB: 2FO0¹⁰). The c-Abl core is composed of a myristoylated (Myr) N-cap, followed by the SH3, SH2, and kinase domains. The unstructured part of the N-cap that extends to the C-lobe of the kinase domain is represented as a dotted line. The SH2-kinase linker forms a polyproline type II helix that engages the SH3 domain. (B) Positions of activating mutations of the c-Abl core used in this study. These include isoleucine substitution of the Thr315 gatekeeper position in the kinase domain (T315I), asparagine substitution of Ala356 (A356N) in the kinase domain C-lobe pocket that engages the myristoylated N-cap, and glutamic acid replacement of two prolines in the SH2-kinase linker (P242, P249), which were combined with deletion of N-cap residues 1–82 in the Δ Ncap-2PE mutant.

of these domains as a function of kinase activation is less clear. A single-crystal structure of c-Abl that was activated by removal of all regulatory constraints revealed dramatic repositioning of the SH2 domain to the top of the kinase domain N-lobe (Nagar et al., 2003; PDB: 1OPL, molecule B¹¹), a result supported by other solution-based biophysical measurements.⁸ These structural rearrangements correlate with a large increase in kinase activity, which is consistent with the loss of these key regulatory domain contacts with the back of the kinase domain.

Another attractive approach to investigate Abl structure is X-ray solution scattering, which enables structural characterization of protein forms that are not amenable to crystallization.^{13–16} In particular, flexible conformations of large structures with multiple domains can be readily analyzed with this technique. Ensembles containing multiple conformational states may be identified from X-ray scattering patterns, as has been shown for the Src-family kinase Hck, which has a similar array of regulatory domains as Abl.¹⁷ In addition to well-known structural measures such as the radius of gyration (R_g) of the molecules in a sample, methodology for the *ab initio* calculation of low-resolution three-dimensional molecular envelopes from intensity data has become well-established.¹⁶ This approach to determination of molecular envelopes is attractive because the shapes of the reconstructed molecular envelopes are independent of any specific, previously known atomic model.

Using the same hyperactive c-Abl protein (PDB: 1OPL, molecule B¹¹) where SH2 was observed to be positioned on the top on the kinase domain's N-lobe by X-ray crystallography, a

molecular envelope was obtained by small-angle X-ray solution scattering. The conformation of Abl from those measurements yielded a fully extended conformation with the kinase, SH2, and SH3 domains in a linear arrangement, although the precise location of SH3 was not resolved.¹⁰ Between the inactive assembled state and this fully disassembled state, X-ray solution scattering data from an SH2 mutant of the hyperactive construct identified an intermediate state (or set of states) that has resisted a specific structural interpretation.¹⁰ In complementary studies, NMR analysis showed that when the ATP-site inhibitor imatinib is bound to the Abl kinase domain the structure becomes more dynamic with respect to the SH2 and SH3 domains.¹⁸ Taken together, these studies demonstrate remarkable dynamic interplay between the c-Abl regulatory and catalytic domains, which raises the important question of the ensemble of possible active states attainable. Despite intense research efforts, our understanding of the structural transitions between the active and inactive states of c-Abl and the mechanisms that determine the equilibrium between them remains incomplete.

To characterize the range of active conformational states attainable by the c-Abl kinase, we created four recombinant c-Abl core proteins that model a graded range of active states. This approach allowed us to sample the core conformation at various points along the activation coordinate, in contrast to previous approaches that focused on the highly active form described above that lacks the N-cap and a functional linker and adopts an extended conformation. X-ray scattering was used to determine the solution structures of these proteins, which included (1) the wild-type (WT) myristoylated c-Abl kinase core protein, identical in amino acid sequence to the one for which the crystal structure was solved by Nagar et al.,^{10,11} (2) an alanine to asparagine point mutant in the myristic acid-binding pocket of the kinase domain's C-lobe (A356N), which interferes with insertion of the myristate group of the N-cap necessary for kinase downregulation;¹² (3) an imatinib-resistant mutant in which the gatekeeper threonine is substituted with isoleucine (T315I);⁶ and (4) a double mutant lacking a portion of the N-cap (amino acids 1–82) that includes the myristoylation site plus dual proline to glutamate substitutions in the SH2-kinase linker (prolines 242 and 249) that disrupt intramolecular docking of the SH3 domain (Δ Ncap-2PE).^{10,11} The positions of these mutations are modeled on the crystal structure of the downregulated c-Abl core in Figure 1B. These kinase proteins span a broad range of intrinsic catalytic activities, with the following rank order: WT < A356N < T315I < Δ Ncap-2PE. Our X-ray scattering results demonstrate that activation of the c-Abl kinase domain does not necessarily require regulatory domain displacement or destabilization of the assembled core structure associated with downregulation. However, the clinically important imatinib-resistance T315I mutation causes an unexpected and dramatic rearrangement of the overall core structure, providing new insight into its heightened catalytic and signaling capabilities.

EXPERIMENTAL PROCEDURES

Protein Expression and Activity Measurements.

Construction of baculovirus vectors for insect cell expression of the Abl core proteins used in this study has been described elsewhere.^{10,19} The Abl high-affinity linker (HAL) sequence used is -RNPPPPYPPSPNYDKMW-, where the five proline substitutions are underlined; this mutant corresponds to HAL9 in Panjarian et al.¹⁹ For protein production, Sf9 cells were

coinfecting with Abl core and YopH phosphatase baculoviruses to allow purification in the dephosphorylated state.¹⁹ Abl proteins were purified from infected cell lysates using a combination of ion exchange and affinity chromatography and dialyzed against 20 mM Tris-HCl (pH 8.3) containing 100 mM NaCl and 3 mM DTT. Purity and mass of each purified protein were verified by SDS-PAGE and mass spectrometry. Tyrosine kinase activity of recombinant Abl core proteins was assessed using the FRET-based Z'Lyte kinase assay system and Tyr-2 peptide substrate, as described elsewhere.⁸

In Vitro Kinase Assay. The specific activity of each recombinant Abl core protein was determined using the FRET-based Z'Lyte *in vitro* kinase assay and Tyr2 peptide substrate (ThermoFisher), as described elsewhere.⁸ Briefly, the Tyr2 peptide is tagged with coumarin and fluorescein on its N- and C-terminus, respectively, to form a FRET pair, and the emission ratio of the coumarin to fluorescein (FRET) fluorescence serves as the readout. After phosphorylation by Abl, a site-specific protease is added, resulting in selective cleavage of the unphosphorylated peptide and loss of the FRET signal. Kinase assays were performed in 384-well black microplates according to the manufacturer's instructions. Each Abl protein was titrated into the assay over a concentration range of 0.2–200 ng/well. Reactions were initiated by the addition of ATP (50 μ M) plus Tyr2 peptide substrate (1 μ M) and incubated for 1 h, followed by addition of the development protease. The assay included a 0% phosphorylation control with unphosphorylated peptide and no kinase and a 100% phosphorylation control with stoichiometrically phosphorylated Tyr2 peptide. Coumarin and fluorescein fluorescence were measured on a Molecular Devices SpectraMax M5 microplate reader, and the results are expressed as percent of maximum kinase activity relative to the control peptides.

Differential Scanning Fluorimetry (DSF). DSF measurements were performed using a StepOnePlus real-time quantitative PCR instrument (Applied Biosystems) and software (version 2.3). DSF assays (20 μ L) were run in duplicate in sealed MicroAmp Fast 96-well qPCR plates (Applied Biosystems). DSF profiles were acquired with recombinant Abl core proteins (2 μ M) in bicine buffer (10 mM bicine, 150 mM NaCl, pH 8.0) and SYPRO Orange (Sigma) diluted to a 5 \times working concentration. Parallel reactions without proteins were run to correct for background fluorescence. DSF reactions were allowed to equilibrate to 25 $^{\circ}$ C for 2 min, followed by an increase to 99 $^{\circ}$ C at a 1% temperature ramp rate (1.6 $^{\circ}$ C/min) with continuous data collection. Background fluorescence was subtracted, and mean fluorescence intensities were then plotted as a function of temperature. Melt curves were fit using the Boltzmann sigmoid function of GraphPad Prism 6, and T_m values were calculated as the midpoint of the thermal transition between the minimum and maximum fluorescence intensities.

X-ray Solution Scattering Data Collection. Small-angle X-ray scattering (SAXS) data (run 1) were collected using undulator-based beamline X9 at the National Synchrotron Light Source (NSLS) at Brookhaven National Laboratory configured with two detectors²⁰ to collect both SAXS and wide-angle X-ray scattering (WAXS) data simultaneously, over the range of $0.01 < q < 2.0 \text{ \AA}^{-1}$, where q is the momentum transfer ($q = 4\pi \sin(\theta)/\lambda$), 2θ is the scattering angle, and λ is the wavelength of incident X-rays. Data were collected at an X-ray wavelength of 0.9184 \AA . Additional data sets were subsequently collected over the resolution range $0.008 < q < 1.75 \text{ \AA}^{-1}$ (run

2) to provide information on the Δ Ncap-2PE construct and facilitate control calculations. Data were collected at ~ 2 and ~ 4 mg/mL for all constructs except Δ Ncap-2PE, which were collected at ~ 1.4 mg/mL. These data, other data sets, and previous work⁹ show an absence of concentration-dependent effects in this regime. A Photonic Science CCD detector operated as the WAXS detector, and a Mar 165 CCD, as the SAXS detector. The SAXS detector was located 3.4 m from the sample. Samples were loaded into a 96-well plate and aspirated into the 1.5 mm diameter, thin-walled sample tube using an automated system previously described.²⁰ Preliminary data processing was carried out using the X9 software package to produce circularly averaged intensity profiles combining data from the two detectors and extending over the entire range of q values. The processed data were examined using the display programs in the ATSAS program suite.²¹

Reconstruction of Molecular Envelopes. Reconstructions of molecular envelopes from X-ray solution scattering data were performed using programs from the ATSAS software suite.²¹ The particle distance distribution function, $P(r)$, was calculated using GNOM²² with data resolution limits and the maximum allowed interatomic distance, r_{max} selected empirically to optimize the fit to the intensity data. In addition to scoring trials for $P(r)$ using the output from GNOM, the shape of $P(r)$ and the reciprocal space fit of the transform of $P(r)$ to the observed data were also checked by visual inspection.

Three-dimensional models of connected beads were generated to fit the data using GASBOR,¹⁶ with the number of beads set approximately equal to the number of amino acids in the Abl constructs. Between 10 and 40 independent modeling runs were performed on each data set, depending on the consistency of solutions and, for key selected examples, to assess the reproducibility of features in the molecular envelopes by comparing subaverages from the replicated GASBOR calculations. Grid objects and molecular surfaces corresponding to Abl molecular envelopes were obtained by aligning the replicated bead models with the DAMSEL and SUPCOMB²³ programs. A locally developed program was used to convert these sets of aligned bead models to contiguous grid objects in which the volumes filled by the molecular envelope are represented by a set of pseudoatoms set on a cubic grid with a 4 \AA interval. This program facilitates examinations of the distribution and population density of beads within sets of aligned bead models to help ensure that the final reconstruction represents a sufficiently converged average. For the six reconstructions carried out on the initial data collection run (run 1), the grid objects were generated by counting the number of aligned beads within 8 \AA of each grid point and thresholding these number densities to give objects with approximately the same partial specific volume as that calculated from the Abl sequence. The reconstructions for the four data sets collected in the second run (run 2) showed somewhat more scatter, so the larger range of 16 \AA was used to calculate bead number densities to obtain an appropriately smooth molecular envelope.

Fits of molecular envelopes onto protein atomic structures of Abl were performed interactively with the molecular graphics program MIFit (<https://github.com/mifit/mifit>) and by automated shape matching with SUPCOMB. Available atomic structures for the Abl constructs are the compact, inactive form exemplified by PDB entry 2FO0 and a partial structure (missing the SH3 domain) of a more extended conformation that is available as PDB entry 1OPL, molecule B.

The high-affinity linker Abl construct known as HAL9¹⁹ served as a useful operational control for the *ab initio* envelope determination protocols because this form was designed with a high-affinity linker that maintains the compactness of the inactive structure obtained by crystallography (PDB: 2FO0). Biophysical data indicate that the impact of additional mutations (A356N or T315I) is largely suppressed by the HAL9 sequence. Consistent with these expectations and intensity data (Figure 3A), we observed that all three *ab initio* shape reconstructions for the HAL9 constructs are very similar to each other and make an excellent match to this crystal structure (see Results). The fidelity of these fits indicates that our experimental data and reconstruction protocols are robust and reliable.

Surface Plasmon Resonance (SPR). Interactions of the Abl core proteins with the SH3-binding peptide p41 (amino acid sequence PPPPPSYSP)²⁴ were analyzed at 25 °C using a Reichert SR7500DC two-channel SPR instrument and a carboxymethyl dextran hydrogel biosensor chip (Reichert Technologies). The p41 peptide was biotinylated on its N-terminus using NHS-PEG₄-biotin (ThermoFisher) prior to immobilization. The carboxymethyl group on the biosensor chip was activated with a mixture of *N*-(3-(dimethylamino)propyl)-*N'*-ethylcarbodiimide hydrochloride and *N*-hydroxysuccinimide (Sigma-Aldrich), followed by immobilization of avidin (ThermoFisher). The biotinylated p41 peptide was injected onto the avidin surface on the left channel and immobilized to a level of 200 response units (μ RU), whereas the right channel was used as a reference for nonspecific binding of Abl proteins to the avidin surface. Abl proteins were analyzed over a range of concentrations (0.1–3.3 μ M) in running buffer (20 mM Tris-HCl, pH 8.3, 150 mM NaCl, 3 mM DTT, 0.05% Tween 20). Each protein was injected in triplicate over the p41 peptide and reference channels at a flow rate of 30 μ L/min. Association was measured for 60 s, followed by a 180 s dissociation phase in running buffer. For the interaction of the WT, T315I, and A356N Abl core proteins with p41, the chip surface was regenerated with running buffer. For the interaction of Abl Δ Ncap-2PE, the sensor surface was regenerated by injecting 5 mM NaOH for 1 min after each run to ensure complete dissociation of bound protein. In addition to reference channel subtraction, running buffer-only cycles were used to allow double referencing for all analyses. Sensorgrams were fit to a simple 1:1 Langmuir interaction model ($A + B \rightleftharpoons AB$) using the data analysis program TraceDrawer 1.6.1 (Reichert).

RESULTS

Expression and Biochemical Characterization of c-Abl Kinase Core Proteins. The recombinant c-Abl core proteins were expressed in Sf-9 insect cells and purified to homogeneity, and their masses and post-translational modifications (myristoylation and phosphorylation) were confirmed by mass spectrometry. In all cases, the mass spectra were indistinguishable from those previously reported for each of these proteins.^{8,19} Additional constructs incorporating a high-affinity linker sequence (HAL9)¹⁹ that stabilizes intramolecular binding to the SH3 domain were expressed as controls. Using an *in vitro* kinase assay,⁸ we determined the concentration of each Abl kinase required for 50% maximal substrate phosphorylation (EC_{50}) as a relative measure of intrinsic protein kinase activity. As shown in Figure 2A, the kinases spanned a wide range of activities, with the WT (least active) and Δ Ncap-2PE (most

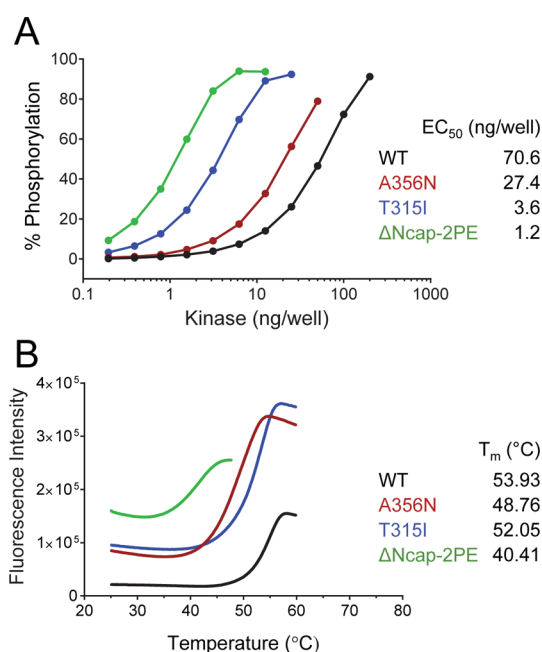


Figure 2. Activity and thermal stability measurements for recombinant Abl core proteins. (A) *In vitro* kinase assays of recombinant purified Abl core proteins. Kinase activity was determined using a FRET-based tyrosine kinase assay with a peptide substrate and increasing amounts of each recombinant Abl protein. Each condition was repeated in quadruplicate, and the extent of phosphorylation is expressed as the mean percentage phosphorylation relative to a control phosphopeptide \pm SD. Each kinase activation curve was best-fit by nonlinear regression analysis, and the resulting EC_{50} values for half-maximal kinase activity are shown. (Note that the SD values are smaller than the diameter of the symbols; therefore, the error bars cannot be seen.) (B) Differential scanning fluorimetry (DSF) assay. DSF was performed on the four Abl core proteins shown, as described in the Experimental Procedures. Background-corrected fluorescence intensities for each protein are plotted as a function of temperature for a representative assay. Temperatures at which half-maximal fluorescence were observed (T_m values) are indicated on the right.

active) differing by nearly 60-fold. The A356N and T315I mutants exhibited intermediate activities, consistent with previous studies in cell-based assays.¹⁹ We then compared the thermal stability of each protein using a DSF assay.²⁵ Each purified Abl protein was gradually heated in a quantitative PCR instrument in the presence of the reporter dye, SYPRO Orange. As the temperature rises and the protein unfolds, the reporter dye gains access to the hydrophobic interior of the protein, resulting in an increase in dye fluorescence. The resulting rise in fluorescence as a function of temperature eventually reaches a maximum, and the resulting protein “melt curve” is fit by nonlinear regression analysis to obtain a T_m value (temperature at which half-maximal thermal denaturation is observed). As shown in Figure 2B, the T_m values for the WT (assembled) core and the fully disrupted Δ Ncap-2PE mutant varied by more than 13 °C. This large decrease in the T_m of the Δ Ncap-2PE mutant relative to WT is consistent with the loss of regulatory constraints and a resulting increase in dynamic behavior. The myristate binding pocket mutant (A356N), on the other hand, showed only a 5 °C reduction in thermal stability relative to WT, consistent with the more modest enhancement of kinase activity compared to that of Δ Ncap-2PE. Remarkably, the T315I gatekeeper mutant showed a reduction in T_m of less than 2 °C relative to WT, suggesting that this mutant adopts a

thermally stable albeit more active conformation. X-ray scattering data presented in the next section support this idea.

X-ray Scattering Analysis. We next collected SAXS and WAXS data under a consistent set of conditions from each of the Abl core constructs. Plots of the X-ray intensities as a function of q show continuous changes in intensities with little indication of jitter across adjacent data points that would indicate significant random noise (Figure 3). Calculations of R_g obtained using GNOM show that the average solution

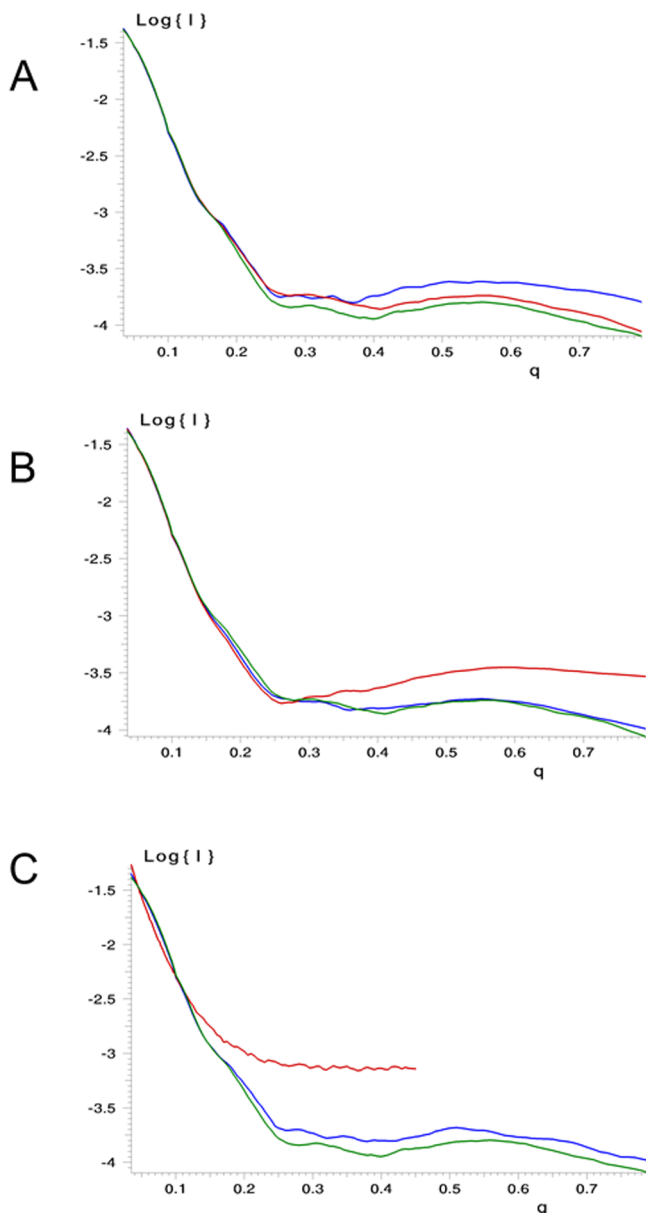


Figure 3. Plots of X-ray intensities, I , as a function of resolution, q . (A) Comparison of intensity data for the three constructs that include the HAL9 sequence (green), HAL9 + T315I (blue), and HAL9 + A356N (red). (B) Comparison of intensity data for WT (blue) and the A356N mutation (red) with the HAL9 data shown for comparison (green). (C) Comparison of intensity data for the T315I mutation (blue), the Δ Ncap-2PE construct (red), with data for the most compact structural form, HAL9, shown for comparison (green). Since the SH2 and SH3 domains in the Δ Ncap-2PE construct are radically repositioned compared to their locations in the other constructs, the resulting scattering curve has a distinctly different appearance.

structures of the WT and A356N proteins are the nearest to that expected for a spherical protein, whereas R_g values from T315I and Δ Ncap-2PE correspond to shapes that are significantly more elongated (Table 1). The rank order of R_g

Table 1. Radii of Gyration for Recombinant Abl Core Proteins^a

| Abl protein | R_g (Å) |
|-------------------|-----------|
| A356N | 27.7 |
| WT | 28.1 |
| T315I | 28.7 |
| Δ Ncap-2PE | 39.4 |
| HAL9 | 26.8 |
| HAL9 + A356N | 27.1 |
| HAL9 + T315I | 27.1 |

^aRadii of gyration, R_g , were calculated from X-ray scattering curves by the GNOM program²² from the resulting pair distribution function, $P(r)$.

for these samples is WT \approx A356N < T315I \ll Δ Ncap-2PE, which correlates closely with their intrinsic protein tyrosine kinase activity ranking (Figure 2A). The smallest values for R_g were obtained for the three constructs that included the high-affinity linker (HAL9) sequence,¹⁹ consistent with the role of SH3–linker interaction in stabilizing the assembled structure of the downregulated kinase. Similar estimates of R_g were obtained from linear fits of Guinier plots (Figure S1). Consistent with these differences in R_g , the shape of the particle distance distribution function, $P(r)$, for the T315I sample is noticeably different from the shapes of $P(r)$ obtained from other comparable constructs (Figure S2). The $P(r)$ derived from our data on the structurally distinct hyperactive construct, Δ Ncap-2PE, is similar in shape to the image presented in a previous study,¹⁰ with a unique form that is indicative of a more extended molecular envelope.

The values of R_g obtained from our experiments also compare favorably with published results of $R_g = 27.2$ Å for the compact, inactive WT form and $R_g = 31.7$ Å for a structurally undetermined active form that may contain multiple active conformational states.¹⁰ The fully extended Δ Ncap-2PE construct exhibits an $R_g = 39.4$ Å, significantly larger than the R_g value of 34.5 Å obtained for a similar construct reported in an earlier study.⁹ A conformational form consisting of a linear array of structural domains might be expected to exhibit some flexing between domains, and our observation of a larger R_g in the absence of a stabilizing small molecule inhibitor PD166326 (used in the earlier work) suggests that the ligand may well impact the relative positions of domains in the extended configuration.

Kratky plots (i.e., plots of $I \cdot q^2$ versus q) provide a qualitative tool for assessing whether protein in a solution scattering sample is folded, flexible, or compactly folded and well-ordered.²⁶ As is characteristic of compactly folded proteins, plots from all constructs (Figure 4) show a significant peak at low q that diminishes as q approaches 0.3 \AA^{-1} and then slowly rises. Remarkably, the Kratky plot for the T315I mutant is very similar to that of WT over the entire range of q values, suggesting that this mutation does not impart a substantial increase in flexibility despite its strong effect on kinase activity (Figure 2A). This result is consistent with the thermal melt data, which shows only slightly higher T_m for WT than T315I (Figure 2B). The Kratky plot for the HAL9 protein indicates

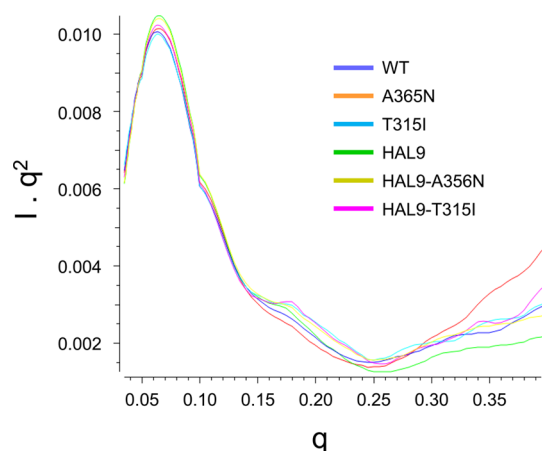


Figure 4. Kratky plots for Abl samples. Results from six Abl protein samples collected under the same experimental conditions are shown. The scattering curves are normalized to place them on a common scale.

that this is the most rigid structure, consistent with the original design goal of creating a high-affinity linker to enhance internal docking to the SH3 domain.¹⁹ Remarkably, addition of mutation T315I or A356N to the HAL9 construct had relatively little impact on the shape of the curve, consistent with the dominant role of the HAL9 linker sequence in these constructs. The largest differences displayed in the Kratky plots are in the range of $q > 0.25 \text{ \AA}^{-1}$ between the data set obtained from HAL9, which is expected to be the most rigid structural variant, and the A356N myristic acid binding pocket mutant, in which perturbation of myristoylated N-cap packing across the protein may result in more conformational freedom. The X-ray scattering curves obtained from these two samples are separated by ~ 3 standard deviations in the higher- q section of the Kratky plot. Differences in Kratky plots from these two samples may therefore reflect the lower stability of the A356N mutant. Further support for the view that the scattering differences highlighted by the Kratky plots are indicative of greater conformational freedom for the A356N Abl molecule comes from scattering data of a related mutant lacking the N-terminal glycine required for addition of myristic acid (G2A mutant). Without N-terminal myristoylation, the N-cap cannot engage the C-lobe of the kinase domain, resulting in a more relaxed conformation with enhanced kinase activity. Data from the Abl G2A mutant display even greater scattering in the high- q region of the Kratky plot than that observed for the A356N

mutant (not shown). These structural forms are discussed in more detail in the next section.

Shape Reconstructions from X-ray Solution Scattering Data. Reconstructions of the molecular envelopes of each Abl structure from solution X-ray scattering were performed using standard methods (Table 2) to identify distinct conformational states and to compare these states with the available Abl crystal structures. Conclusions regarding the relative similarities of the reconstructed molecular envelopes to each other were checked by calculation of overlaps with the SUPCOMB program.²³ Insights regarding the solution structure of each Abl core protein resulting from these reconstructions are summarized below.

Wild-Type and A356N Myristic Acid Binding Pocket Mutant. Reconstructions of the protein shapes from the WT Abl core protein and the A356N myristic acid binding pocket mutant differ only slightly from one another and also agree quite well with the crystal structure of the inactive conformation (PDB: 2FO0; Figure 5A,B). Previously reported solution scattering data collected from a WT Abl sample containing a stabilizing ligand also resulted in a shape consistent with this crystal structure.¹⁰ Although the A356N mutation enhances the intrinsic kinase activity of Abl both *in vitro* (Figure 2A) and in cells,¹⁹ the shape of this reconstruction suggests that this mutation induces an active conformation without movement of the SH2 to the so-called “top-hat” position, where it engages the kinase domain’s N-lobe and stabilizes an active conformation of the kinase domain.²⁷ This conclusion is supported by previous results from hydrogen exchange mass spectrometry, which revealed that an identical A356N Abl core protein shows very little difference in deuterium uptake relative to the WT form.¹⁹ These results imply that activation of Abl by displacement of the myristate group from N-lobe may result in an active state in which the core retains the assembled configuration. Indeed, incubation of WT Abl with the small molecule DPH [5-(1,3-diaryl-1H-pyrazol-4-yl)hydantoin], which binds to the myristic acid binding pocket and causes Abl activation,²⁸ had no effect on the overall shape of the WT Abl core envelope (Figure S3).

Hyperactive Δ Ncap-2PE Mutant. Analysis of scattering data from the active Δ Ncap-2PE construct revealed a molecular envelope with a highly elongated appearance, as expected from its R_g and consistent with earlier work¹⁰ (Figure 5C). The SAXS data previously obtained from this construct were pivotal for developing the standard model for conformational change in Abl activation. The prior study modeled the Δ Ncap-2PE

Table 2. Data Sets and Parameters for the Reconstruction of Molecular Envelopes^a

| run | sample | resolution range, $q \text{ (\AA}^{-1}\text{)}$ | R_{max} (Å) | no. of reconstruction runs | clustering score (NSD) |
|-----|-------------------|---|----------------------|----------------------------|------------------------|
| 1 | A356N | 0.035–0.80 | 85 | 10 | 1.024 |
| 1 | WT | 0.035–0.80 | 85 | 10 | 1.125 |
| 1 | T315I | 0.035–0.80 | 85 | 10 | 1.171 |
| 1 | HAL9 | 0.011–0.80 | 80 | 10 | 1.103 |
| 1 | HAL9 + A356N | 0.010–0.80 | 80 | 10 | 1.096 |
| 1 | HAL9 + T315I | 0.035–0.80 | 80 | 10 | 1.029 |
| 2 | Δ Ncap-2PE | 0.035–0.45 | 115 | 40 | 2.009 |
| 2 | HAL9 | 0.028–0.49 | 80 | 40 | 1.192 |
| 2 | T315I | 0.035–0.80 | 80 | 40 | 1.488 |
| 2 | WT | 0.035–0.80 | 85 | 20 | 1.265 |

^aReconstructions were performed with GASBOR,¹⁶ and the resulting bead models were aligned by SUPCOMB.²³ The similarity between aligned bead models with each run is measured by the normalized spatial discrepancy (NSD) for each set as defined by SUPCOMB.

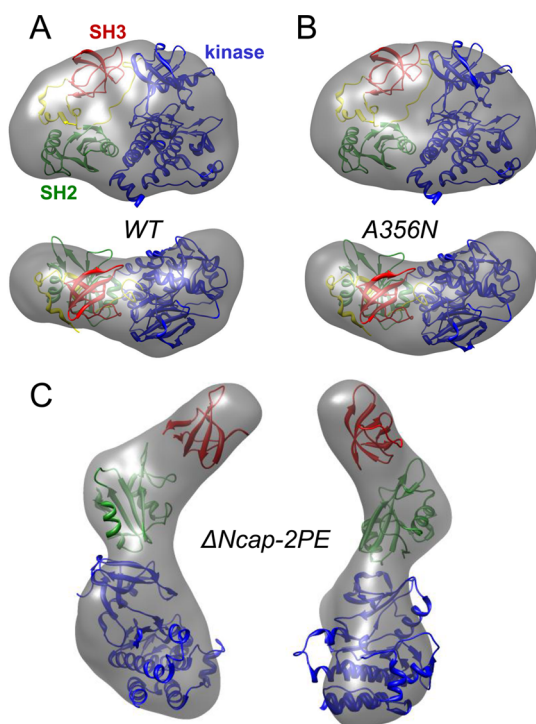


Figure 5. X-ray solution scattering reconstructions for Abl WT, A356N, and Δ Ncap-2PE. The reconstruction volumes are superimposed on the backbone chain traces for the kinase, SH2, and SH3 domains. Two orthogonal views are shown for each example. The best overlap between model and reconstruction in all images was obtained using SUPCOMB,²³ and the images were rendered with MIFit. Reconstructions for (A) wild-type (WT) and (B) A356N mutant Abl core proteins superimposed on the crystal structure of Abl in the inactive form (PDB: 2FO0¹⁰). (C) Reconstruction for the Δ Ncap-2PE mutant protein showing the fit of the kinase and SH2 domains from the disassembled crystal structure (PDB: 1OPL, molecule B), with the SH3 domain fitted to the unfilled volume.

protein using an Abl conformation based on PDB entry 1OPL (molecule B) for the kinase and SH2 domains, with the SH2 domain in the top-hat configuration next to the kinase domain's N-lobe as described above. The SH3 domain was fitted to occupy the remaining empty space adjoining the SH2 domain and extending to the full 115 Å length of the molecular envelope. The surface of our reconstruction more clearly defines the separate domains of this extended structural arrangement, with a narrowing of the protein envelope at the boundaries of the kinase, SH2, and SH3 domains.

T315I Imatinib-Resistant Gatekeeper Mutant. The shape of the T315I reconstruction is markedly different from that of the downregulated WT Abl core as well as the active A356N and Δ Ncap-2PE mutants. The T315I molecular envelope tends toward a “squashed pear” form that is poorly fit by the complete crystal structure of the inactive conformation, as exemplified by PDB entry 2FO0 (Figure 6A). These data strongly suggest that this single-drug-resistance mutation in the kinase domain has profound allosteric effects on the overall shape of the Abl core. This previously unobserved active state of Abl may contribute to the unique kinetic properties and altered substrate selection profile of the T315I mutation in the context of Bcr-Abl.⁷ These data are also consistent with previous hydrogen exchange studies, which revealed subtle increases in SH3 domain deuterium uptake in the T315I mutant compared to that in WT Abl.⁸ In order to confirm this

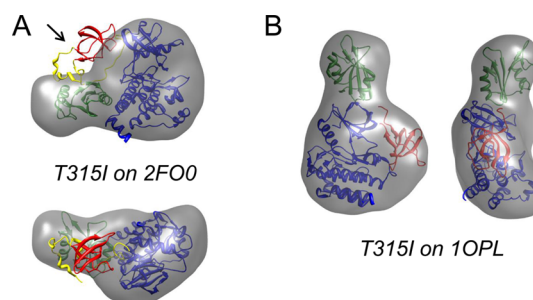


Figure 6. X-ray solution scattering reconstructions for the Abl core protein bearing the imatinib-resistance mutation, T315I. (A) Reconstruction of the T315I gatekeeper mutant superimposed on the crystal structure of the assembled Abl core (PDB: 2FO0). Note that the T315I scattering envelope is fit poorly by the 2FO0 structure, leaving the position of the SH3 domain unaccounted for (arrow). (B) Superposition of the T315I envelope on the extended conformation of an active Abl structure (PDB: 1OPL, molecule B¹¹). The SH3 domain was manually fit in the remaining void adjacent to the kinase domain.

unexpected conformation of the T315I mutant, an independent data set was obtained with a second preparation of T315I (Figure S4, run 2) and generated essentially identical results.

One possible explanation for the squashed pear shape observed for T315I is that the SH3 domain in the T315I mutant is insufficiently ordered to be represented by the bead models obtained during reconstruction calculations and does not contribute to the final image of the protein shape. However, the high T_m (Figure 2D) and Kratky plot (Figure 4) both suggest that T315I Abl is well-folded. Alternatively, the T315I substitution may trigger a rearrangement of the SH2 and SH3 domains. One possibility, consistent with our data, is that observed in PDB entry 1OPL (chain B),¹⁰ in which the SH2 domain is juxtaposed to the kinase domain's N-lobe (Figure 6B). The SH3 domain was not visualized in this crystal structure, but if the SH2-kinase linker is refolded, the remaining unfilled space in the envelope can be fit by the SH3 domain.

Enhanced SH3-Linker Interaction Reverses the Structural Changes Induced by the T315I Mutation. Recent work by Panjarian et al. has shown that the strength of intramolecular SH3 domain interaction with the SH2-kinase linker has a dominant effect on Abl kinase activity and Bcr-Abl kinase inhibitor sensitivity.¹⁹ This study reported a series of Abl and Bcr-Abl proteins with modified SH2-kinase linkers containing extra proline residues to enhance internal SH3 docking. The HAL9 linker, described above, has five linker proline substitutions that reverse the activating effects of both the A356N and T315I mutations in cell-based assays.¹⁹ These observations predicted that X-ray scattering studies of the HAL9 forms of our active Abl mutants may show a return to the assembled inactive state associated with the crystal structure of the WT Abl core. To test this idea, we expressed and purified HAL9 versions of the Abl core protein on the WT, A356N, and T315I backgrounds. X-ray scattering data were then collected on each of these proteins and compared to results with the complementary constructs with WT linkers (Figure 7).

The shape of the reconstruction from the HAL9 construct that is otherwise WT (Figure 7A) is completely consistent with the crystal structure of the WT Abl core in the assembled inactive conformation (PDB: 2FO0¹⁰). This result indicates that the introduction of five additional linker prolines enhances SH3 engagement without distorting the overall shape of the downregulated molecule. Intensity data and the resulting

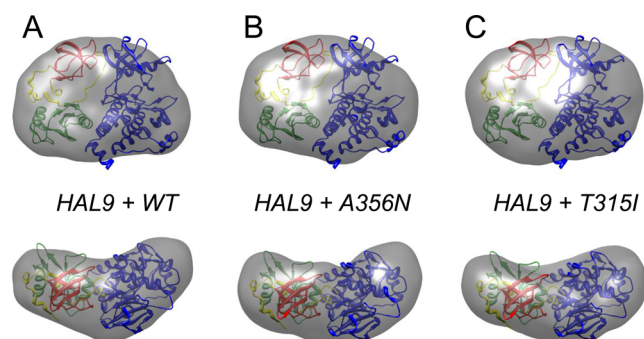


Figure 7. X-ray solution scattering reconstructions for the Abl core proteins bearing high-affinity linker (HAL) substitutions. Scattering envelopes for the HAL9 variants of wild-type (WT), A356N, and T315I Abl core constructs superimposed on the downregulated Abl structure (PDB: 2FO0¹⁰).

reconstruction of the HAL9 variant of the A356N protein (Figure 7B) are also indistinguishable from those obtained for the HAL9 construct with a WT kinase domain. This observation is fully consistent with previous hydrogen exchange data showing that subtle dynamic changes resulting from the A356N mutation are abolished by incorporation of this high-affinity linker sequence.¹⁹ Remarkably, the intensity data and molecular reconstruction from the HAL9 protein incorporating the T315I mutation (Figure 7C) are also very similar to those obtained from the control HAL9 construct. This result indicates that enhanced SH3–linker interaction overrides the dramatic structural rearrangement triggered by the T315I mutation (Figure 6). Similarly, the compact shape of the HAL9 variant of the T315I protein is consistent with the observation that the enhanced activity of the T315I mutant is suppressed in cells when coupled to the HAL9 sequence.¹⁹ The shape reconstructions for the three HAL proteins are also consistent with the R_g values, which are all smaller than the value observed for WT Abl (Table 1).

SH3 Domain Accessibility Is Enhanced in Δ Ncap-2PE but Unaffected in the WT, A356N, or T315I Abl Core Proteins. In a final series of experiments, we investigated whether the activating mutations to the Abl core impacted the ability of their SH3 domains to bind to a ligand in trans. For these studies, we employed a surface plasmon resonance approach using a short proline-rich peptide, known as p41, as the SH3 ligand. Previous studies have shown that the p41 peptide interacts with the isolated Abl SH3 domain in the low micromolar range, and X-ray crystallography shows that it adopts the polyproline type II helical conformation associated with most SH3 ligands.^{24,29} The p41 peptide was immobilized on the biosensor surface, and interaction of each of the Abl core proteins was then monitored in real time. As shown in Figure 8, the Δ Ncap-2PE protein interacted readily with this SH3-binding peptide in a concentration-dependent manner, yielding a K_D value of $3.4 \pm 0.2 \times 10^{-7} \mu\text{M}$. This observation is consistent with the SAXS envelope for this protein, which shows that the SH3 domain is fully exposed and available for ligand binding. In sharp contrast, no binding was observed for the other three Abl proteins under identical conditions. For the WT and A356N core proteins, these results suggest that the internal SH3–linker interactions remain intact in solution, consistent with the SAXS data. The SPR data also provide important information about T315I, for which SAXS analysis revealed a novel conformation. Lack of T315I interaction with

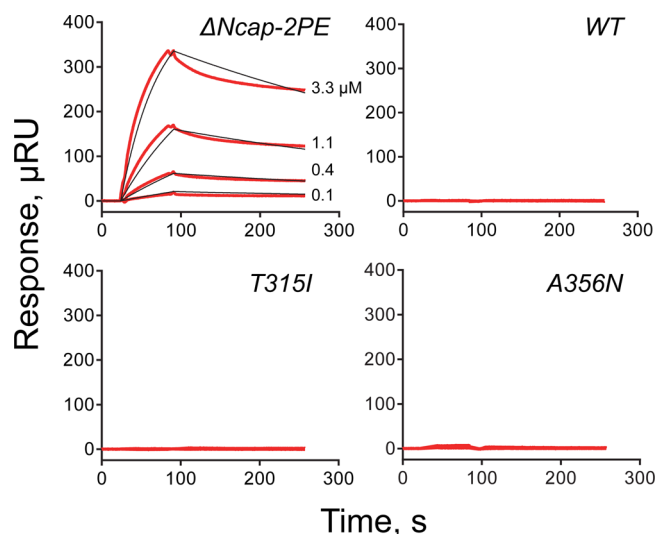


Figure 8. Analysis of SH3 domain accessibility in Abl core proteins by surface plasmon resonance (SPR). The Abl SH3-binding peptide known as p41^{24,29} was biotinylated on its N-terminus and immobilized on an avidin-modified SPR chip surface as described in the Experimental Procedures. Each of the four Abl core proteins shown was injected in triplicate at four different concentrations, and association was monitored for 60 s, followed by a 180 s dissociation phase in running buffer. Interactions observed with the Δ Ncap-2PE Abl core protein (red traces) were fit to a simple 1:1 Langmuir interaction model (fitted lines in black) and yielded a K_D value of $3.4 \pm 0.2 \times 10^{-7} \mu\text{M}$. No interaction was detected with the other three Abl proteins (WT, T315I, and A356N).

the p41 peptide demonstrates that the binding surface of the SH3 domain remains occluded, possibly through interaction with the linker or through new contacts with the kinase domain. Regardless of the actual structure, these data suggest that T315I adopts a stable, active conformation.

DISCUSSION

SAXS analyses of the diverse Abl core constructs presented here reveal a set of closely similar inactive structures that differ in subtle yet important ways and multiple active conformations in which the positions of the SH2 and SH3 domains are reconfigured. Determination of R_g and the shapes of the molecular envelopes reflect the dramatic restructuring that transforms compact conformations into more elongated forms. One possible explanation for the relatively smooth variation of structural parameters among the WT, A356N, and HAL9 proteins is that the differences in observed data correspond not to distinct conformations but rather to differences in conformational equilibria in which two or more conformations are present in different proportions. As the proportion of the larger component increases, the value of R_g estimated from the X-ray data increases. Reconstructions of molecular envelopes from ensembles are difficult to anticipate, but they can be estimated from data simulations if models of the dominant components are available.³⁰

Reconstructions of the most compact forms obtained from constructs incorporating the HAL9 sequence are all well-fit by a crystal structure of the inactive form (PDB: 2FO0¹⁰). We surmise that the set of structural states corresponding to Abl samples containing the HAL9 sequence is highly dominated by this inactive conformation, even when combined with activating mutations at other sites (e.g., A356N and T315I). The role of

the additional prolines engineered into the linker is to provide additional stability for this structural form compared to that of WT. Mimicking their role may represent a promising approach to inhibition of drug-resistant mutants of Abl. The enhancement of natural SH3–linker interaction with small molecules or antibodies may effectively prevent activation of these and other mutant forms of c-Abl and Bcr-Abl.

Data from the T315I and Δ Ncap-2PE proteins are not consistent with a modulation of conformational equilibria. Data collected from the T315I mutant shows that it exhibits a large and unanticipated departure from the inactive conformation. When calculated with GNOM, the value of R_g obtained from the T315I data is slightly lower than the published value obtained from an SH2 mutant of a hyperactive form with “molecular envelopes that resemble Abl^{activated} (viz. Δ Ncap-2PE) although more compact”.¹⁰ When interpreted on the basis of the alternative Abl conformation identified from protein crystallography (PDB: 1OPL, molecule B), the kinase and SH2 domains fit well into the reconstruction but leave a large unfilled volume adjacent to the kinase domain. The volume of this region is approximately the same as that of the SH3 domain (not visible in the crystal), and we suggest that it represents the positioning of the SH3 domain within this structure (Figure 6). This model appears feasible relative to the crystal data since, when modeled in this position, the SH3 domain fits in a volume that is not occupied by other domains in the 1OPL crystal cell, as suggested previously by Nagar et al.¹⁰

An extended arrangement of kinase, SH2, and SH3 domains has also been reported for a crystal structure of the c-Src kinase that models a possible active state.³¹ This c-Src structure is almost the same length as our Abl-T315I reconstruction but fits the contours of the molecular envelope less well than the model based on Abl 1OPL molecule B (data not shown). Nevertheless, the possibility of some conformational flexibility between domains or the mixing of active and inactive T315I populations might make it possible for a model based on the c-Src structure to be consistent with the solution scattering data.

The structure of the highly active protein, Δ Ncap-2PE, is the most divergent from the other structures. The elongated reconstruction derived from the Δ Ncap-2PE scattering data is consistent with previous results that associated a highly elongated appearance with this active form of the protein,¹⁰ but it is very different from that of T315I despite the high intrinsic kinase activities of both proteins. Our surprising observation that the SH3 domain of Δ Ncap-2PE is freely available for ligand binding in trans whereas the SH3 domain of T315I remains completely occluded supports this view (Figure 8).

In summary, our results show that c-Abl protein tyrosine kinase core studied here can take on at least three distinct active conformations (or families of closely related conformations): a compact active conformation (A356N); a highly elongated, active conformation (Δ Ncap-2PE); and a novel, intermediate active conformation exhibiting a previously unobserved arrangement of regulatory domains (T315I). Abl kinases, and by extension other multidomain kinases including members of the Src and Tec families, may well adopt a wide range of active states in solution. This observation supports a previously unrecognized level of signaling diversity that may be exploitable for therapeutic gain.

■ ASSOCIATED CONTENT

■ Supporting Information

The Supporting Information is available free of charge on the ACS Publications website at DOI: 10.1021/acs.biochem.6b00202.

Guinier plots (Figure S1); particle distance distribution functions (Figure S2); reconstruction of WT Abl protein with small molecule compound DPH (Figure S3); and replicated reconstruction of the molecular envelope of the Abl T315I mutant (Figure S4) (PDF)

■ AUTHOR INFORMATION

Corresponding Author

*Tel. 617-736-3006. E-mail: makowski@ece.neu.edu.

Present Address

#(S.B.P.) Fels Institute for Cancer Research and Molecular Biology, Temple University School of Medicine, 3307 N. Broad Street, Philadelphia, Pennsylvania 19140, United States.

Author Contributions

[†]J.B. and P.G. contributed equally to this work.

Funding

Funding for this work was provided by the National Institutes of Health (CA169962 to T.E.S. and GM101135 to J.R.E.) and a Northeastern University TIER1 grant (J.R.E. and L.M.).

Notes

The authors declare no competing financial interest.

■ REFERENCES

- (1) Colicelli, J. (2010) ABL tyrosine kinases: evolution of function, regulation, and specificity. *Sci. Signaling* 3, re6.
- (2) Hantschel, O., and Superti-Furga, G. (2004) Regulation of the c-Abl and Bcr-Abl tyrosine kinases. *Nat. Rev. Mol. Cell Biol.* 5, 33–44.
- (3) Wong, S., and Witte, O. N. (2004) The BCR-ABL story: bench to bedside and back. *Annu. Rev. Immunol.* 22, 247–306.
- (4) Druker, B. J. (2004) Imatinib as a paradigm of targeted therapies. *Adv. Cancer Res.* 91, 1–30.
- (5) Schindler, T., Bornmann, W., Pellicena, P., Miller, W. T., Clarkson, B., and Kuriyan, J. (2000) Structural mechanism for STI-571 inhibition of abelson tyrosine kinase. *Science* 289, 1938–1942.
- (6) Gorre, M. E., Mohammed, M., Ellwood, K., Hsu, N., Paquette, R., Rao, P. N., and Sawyers, C. L. (2001) Clinical resistance to STI-571 cancer therapy caused by BCR-ABL gene mutation or amplification. *Science* 293, 876–880.
- (7) Griswold, I. J., MacPartlin, M., Bumm, T., Goss, V. L., O'Hare, T., Lee, K. A., Corbin, A. S., Stoffregen, E. P., Smith, C., Johnson, K., Moseson, E. M., Wood, L. J., Polakiewicz, R. D., Druker, B. J., and Deininger, M. W. (2006) Kinase domain mutants of Bcr-Abl exhibit altered transformation potency, kinase activity, and substrate utilization, irrespective of sensitivity to imatinib. *Mol. Cell Biol.* 26, 6082–6093.
- (8) Iacob, R. E., Pene-Dumitrescu, T., Zhang, J., Gray, N. S., Smithgall, T. E., and Engen, J. R. (2009) Conformational disturbance in Abl kinase upon mutation and deregulation. *Proc. Natl. Acad. Sci. U. S. A.* 106, 1386–1391.
- (9) Azam, M., Seeliger, M. A., Gray, N. S., Kuriyan, J., and Daley, G. Q. (2008) Activation of tyrosine kinases by mutation of the gatekeeper threonine. *Nat. Struct. Mol. Biol.* 15, 1109–1118.
- (10) Nagar, B., Hantschel, O., Seeliger, M., Davies, J. M., Weis, W. I., Superti-Furga, G., and Kuriyan, J. (2006) Organization of the SH3-SH2 unit in active and inactive forms of the c-Abl tyrosine kinase. *Mol. Cell* 21, 787–798.
- (11) Nagar, B., Hantschel, O., Young, M. A., Scheffzek, K., Veach, D., Bornmann, W., Clarkson, B., Superti-Furga, G., and Kuriyan, J. (2003)

Structural basis for the autoinhibition of c-Abl tyrosine kinase. *Cell* 112, 859–871.

(12) Hantschel, O., Nagar, B., Guettler, S., Kretzschmar, J., Dorey, K., Kuriyan, J., and Superti-Furga, G. (2003) A myristoyl/phosphotyrosine switch regulates c-Abl. *Cell* 112, 845–857.

(13) Grant, T. D., Luft, J. R., Wolfley, J. R., Tsuruta, H., Martel, A., Montelione, G. T., and Snell, E. H. (2011) Small angle X-ray scattering as a complementary tool for high-throughput structural studies. *Biopolymers* 95, 517–530.

(14) Jacques, D. A., and Trewheella, J. (2010) Small-angle scattering for structural biology—expanding the frontier while avoiding the pitfalls. *Protein Sci.* 19, 642–657.

(15) Hura, G. L., Menon, A. L., Hammel, M., Rambo, R. P., Poole, F. L., Tsutakawa, S. E., Jenney, F. E., Jr., Classen, S., Frankel, K. A., Hopkins, R. C., Yang, S. J., Scott, J. W., Dillard, B. D., Adams, M. W., and Tainer, J. A. (2009) Robust, high-throughput solution structural analyses by small angle X-ray scattering (SAXS). *Nat. Methods* 6, 606–612.

(16) Svergun, D. I., Petoukhov, M. V., and Koch, M. H. (2001) Determination of domain structure of proteins from X-ray solution scattering. *Biophys. J.* 80, 2946–2953.

(17) Yang, S., Blachowicz, L., Makowski, L., and Roux, B. (2010) Multidomain assembled states of Hck tyrosine kinase in solution. *Proc. Natl. Acad. Sci. U. S. A.* 107, 15757–15762.

(18) Skora, L., Mestan, J., Fabbro, D., Jahnke, W., and Grzesiek, S. (2013) NMR reveals the allosteric opening and closing of Abelson tyrosine kinase by ATP-site and myristoyl pocket inhibitors. *Proc. Natl. Acad. Sci. U. S. A.* 110, E4437–E4445.

(19) Panjarian, S., Jacob, R. E., Chen, S., Wales, T. E., Engen, J. R., and Smithgall, T. E. (2013) Enhanced SH3/linker interaction overcomes Abl kinase activation by gatekeeper and myristic acid binding pocket mutations and increases sensitivity to small molecule inhibitors. *J. Biol. Chem.* 288, 6116–6129.

(20) Allaire, M., and Yang, L. (2011) Biomolecular solution X-ray scattering at the National Synchrotron Light Source. *J. Synchrotron Radiat.* 18, 41–44.

(21) Konarev, P. V., Petoukhov, M. V., Volkov, V. V., and Svergun, D. I. (2006) ATSAS 2.1, a program package for small-angle scattering data analysis. *J. Appl. Crystallogr.* 39, 277–286.

(22) Svergun, D. I. (1992) Determination of the regularization parameter in indirect-transform methods using perceptual criteria. *J. Appl. Crystallogr.* 25, 495–503.

(23) Kozin, M. B., and Svergun, D. I. (2001) Automated matching of high- and low-resolution structural models. *J. Appl. Crystallogr.* 34, 33–41.

(24) Pisabarro, M. T., Serrano, L., and Wilmanns, M. (1998) Crystal structure of the abl-SH3 domain complexed with a designed high-affinity peptide ligand: implications for SH3-ligand interactions. *J. Mol. Biol.* 281, 513–521.

(25) Niesen, F. H., Berglund, H., and Vedadi, M. (2007) The use of differential scanning fluorimetry to detect ligand interactions that promote protein stability. *Nat. Protoc.* 2, 2212–2221.

(26) Putnam, C. D., Hammel, M., Hura, G. L., and Tainer, J. A. (2007) X-ray solution scattering (SAXS) combined with crystallography and computation: defining accurate macromolecular structures, conformations and assemblies in solution. *Q. Rev. Biophys.* 40, 191–285.

(27) Filippakopoulos, P., Kofler, M., Hantschel, O., Gish, G. D., Grebien, F., Salah, E., Neudecker, P., Kay, L. E., Turk, B. E., Superti-Furga, G., Pawson, T., and Knapp, S. (2008) Structural coupling of SH2-kinase domains links Fes and Abl substrate recognition and kinase activation. *Cell* 134, 793–803.

(28) Yang, J., Campobasso, N., Biju, M. P., Fisher, K., Pan, X. Q., Cottom, J., Galbraith, S., Ho, T., Zhang, H., Hong, X., Ward, P., Hofmann, G., Siegfried, B., Zappacosta, F., Washio, Y., Cao, P., Qu, J., Bertrand, S., Wang, D. Y., Head, M. S., Li, H., Moores, S., Lai, Z., Johanson, K., Burton, G., Erickson-Miller, C., Simpson, G., Tummino, P., Copeland, R. A., and Oliff, A. (2011) Discovery and character-

ization of a cell-permeable, small-molecule c-Abl kinase activator that binds to the myristoyl binding site. *Chem. Biol.* 18, 177–186.

(29) Pisabarro, M. T., and Serrano, L. (1996) Rational design of specific high-affinity peptide ligands for the Abl-SH3 domain. *Biochemistry* 35, 10634–10640.

(30) Heller, W. T. (2005) Influence of multiple well defined conformations on small-angle scattering of proteins in solution. *Acta Crystallogr., Sect. D: Biol. Crystallogr.* 61, 33–44.

(31) Cowan-Jacob, S. W., Fendrich, G., Manley, P. W., Jahnke, W., Fabbro, D., Liebetanz, J., and Meyer, T. (2005) The Crystal Structure of a c-Src Complex in an Active Conformation Suggests Possible Steps in c-Src Activation. *Structure (Oxford, U. K.)* 13, 861–871.